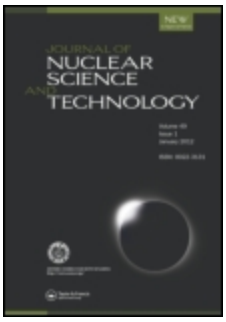

Exact Monte Carlo calculation method for k-eigenvalue change using perturbation source method

Journal:	*Journal of Nuclear Science and Technology*
Manuscript ID	TNST-2020-0266.R1
Manuscript Type:	Article
Date Submitted by the Author:	n/a
Complete List of Authors:	Yamamoto, Toshihiro; Kyoto University, Institute for Integrated Radiation and Nuclear Science Sakamoto, Hiroki; Independent researcher, none
Keywords - Keywords should be the same as those listed on your manuscript title page. Should you have more than 7 words listed in your main document please pick the first 7 :	Monte Carlo, perturbation, reactivity, neutron, cross section
Subject Classification:	304 Neutron Transport Calculation Method and its Application < 3 Reactor Physics, 303 Reactor Analysis Method < 3 Reactor Physics, 302 Reactor Neutronics Design and Characteristics Evaluation < 3 Reactor Physics

Exact Monte Carlo Calculation Method for *K*-eigenvalue Change Using Perturbation Source Method

Toshihiro Yamamoto[a*] and Hiroki Sakamoto[b]

[a]*Institute for Integrated Radiation and Nuclear Science, Kyoto University, 2 Asashironishi, Kumatori-cho, Osaka-fu, Japan;* [b]*Independent researcher, Radiation Dose Analysis and Evaluation Network, 4-13-14, Kokubunji-shi, Tokyo, 185-0001, Japan*

* tyama@rri.kyoto-u.ac.jp

Exact Monte Carlo Calculation Method for *K*-eigenvalue Change Using Perturbation Source Method

The "perturbation source method" (PSM) is a Monte Carlo perturbation method that calculates an exact *k*-eigenvalue change caused by cross-section changes. Although the PSM, which can consider the effect of fission source perturbation, was proposed long ago, it has garnered minimal interest as a Monte Carlo perturbation method. The applicability of the PSM has not been thoroughly elucidated hitherto. This study revisits the PSM and reviews the associated Monte Carlo algorithm. Some improvements have been made to improve the efficiency. The PSM is applied to some numerical tests that involve the replacement of a fuel material with light water, a density change in a water hole, an interface shift between a fuel and reflector, and an external boundary extension. The performance of the PSM for these tests is compared with that of another exact Monte Carlo perturbation method, which is the correlated sampling method. The PSM can yield an accurate *k*-eigenvalue change even for large cross-section changes such as the replacement of a material with another material. The PSM used in this study is the exact method except for the approximation related to the spatial discretization for fission source perturbation. Furthermore, it exhibits superiority in terms of accuracy and computational efficiency, particularly for large perturbations added in a small region.

Keywords: Monte Carlo; perturbation; reactivity; neutron; cross section

1. Introduction

Monte Carlo radiation transport analysis of the effect of small system parameter changes on a response, such as the *k*-eigenvalue, has long been recognized as a formidable challenge. Hence, many studies regarding Monte Carlo perturbation techniques have been performed hitherto [1−14] . The authors of [1] presented a thorough chronological review of the development of Monte Carlo perturbation methods for radiation transport calculations.

According to the review, the correlated sampling method [5, 7, 10, 12], differential operator sampling method [7, 9, 11, 12], and adjoint-based perturbation method [13, 14] are regarded as the primary perturbation calculation methods.

The correlated sampling method (CS) forces particles of perturbed history to follow the same trajectories as those of unperturbed history in the phase space. If CS is applied to calculate a *k*-eigenvalue change, then the effect of perturbation on the fission source must be considered. Nagaya and Mori [12] developed a method to include the effect of fission source perturbation. Although the method does not explicitly rely on the adjoint flux, it is similar to an iterated fission probability method that obtains a quantity proportional to the adjoint flux [13,16–19]. CS with the fission source perturbation effect can yield an exact estimate of the *k*-eigenvalue change. However, one disadvantage of CS is that it entails an unbounded statistical uncertainty for a large perturbation [7, 20, 21]. Hence, the availability of CS may be ambiguous for large perturbations such as material substitution.

The differential operator sampling method (DOS) yields an approximate *k*-eigenvalue change by the Taylor series expansion with respect to a system parameter, such as a cross section. The DOS does not require the calculation of the adjoint flux, and the derivatives of the *k*-eigenvalue with respect to a system parameter can be extended to arbitrary orders [22]. Furthermore, Nagaya and Mori developed a method to implement the effect of fission source perturbation into DOS [12, 22]. The larger the perturbation, the more expansion order is required to obtain a result similar to the exact solution. Furthermore, if several system parameters are perturbed simultaneously, then cross-derivative terms must be considered [23].

The adjoint-based perturbation method [13, 14] yields a *k*-eigenvalue change based on transport perturbation theory [24]. In this method, the product of the cross-section change and the unperturbed flux is adjoint-weighted to estimate the *k*-eigenvalue change due to perturbation. The iterated fission probability (IFP) method is used to obtain adjoint-weighted tallies. Because the method uses unperturbed flux, the results are limited to the first-order

accuracy. As an exceptional example of the exact perturbation method, Truchet et al. [25, 26] developed a two-step method that uses the adjoint-weighted perturbed forward flux. In the first step of the method, a forward eigenvalue calculation is performed for the perturbed system to obtain the perturbed flux. In the second step, an IFP adjoint calculation is performed for the unperturbed system.

The objective of this study is to revisit "the perturbation source method" (PSM), which is an exact Monte Carlo perturbation method for calculating the *k*-eigenvalue change due to perturbation. The PSM has been proposed in several previous studies [3, 4, 6, 8]. Hoffman et al. [4] successfully expanded the capability of PSM to *k*-eigenvalue problems, where the effect of fission source perturbation was considered. However, thereafter, the PSM has garnered minimal interest for decades as a Monte Carlo perturbation method. Therefore, the validity and applicability of the method have not been thoroughly investigated. Recently, the PSM was revisited by Sakamoto and Yamamoto [20, 21] as an exact perturbation method for fixed-source problems. In [20], a new method that introduces pseudo-scattering cross sections was proposed to increase computational efficiency. The applicability and robustness of the PSM for geometry change in fixed-source problems were demonstrated in [21]. Based on these studies regarding the use of the PSM for fixed-source problems, the PSM is expected to be a robust and efficient method for solving *k*-eigenvalue problems. The present study focuses on elucidating the applicability of the PSM to *k*-eigenvalue problems and identifying the advantages and disadvantages of the PSM. In addition, this study aims to implement the pseudo-scattering method and demonstrate its effect.

In Section 2, the theory of the PSM is presented. In Section 3, the Monte Carlo algorithm adopted in this study is described. In Section 4, the results of numerical tests performed are presented. Finally, Section 5 summarizes the performance of the PSM for *k*-eigenvalue problems.

2. Formulation of perturbation source method for *k*-eigenvalue problems

2.1 Perturbation source method without perturbation of fission source

This section presents the fundamental formulation of the PSM that is applicable to perturbation calculations for *k*-eigenvalue changes. Although the underlying concept of the PSM presented herein is essentially similar to that in [4], it is presented differently herein. The formulation presented herein is reconstructed by eliminating the concept of "adjoint" or "importance" that is used in [4], thereby rendering the concept easier to comprehend.

In a *k*-eigenvalue mode calculation, a *k*-eigenvalue is obtained using the power iteration method. Neutrons are started from fission source positions that are inherited from the previous generation. The random walk process is performed by tracking a neutron until its death. The fission neutrons produced during the random walk process are used in the next generation. Regarding the calculation in one generation, the *k*-eigenvalue mode calculation is a fixed source calculation, where the fixed source is the fission source inherited from the previous generation. Subsequently, the neutron transport equation to be solved for a *k*-eigenvalue problem is written in the form of a fixed source problem as follows:

$$\boldsymbol{H}\,\phi(\boldsymbol{r},\boldsymbol{\Omega},E) = \frac{\chi(E)}{4\pi}S(\boldsymbol{r}), \tag{1}$$

where

$$\begin{aligned}\boldsymbol{H}\,\phi(\boldsymbol{r},\boldsymbol{\Omega},E) \equiv\ & \boldsymbol{\Omega}\cdot\nabla\,\phi(\boldsymbol{r},\boldsymbol{\Omega},E) + \Sigma_t(\boldsymbol{r},E)\phi(\boldsymbol{r},\boldsymbol{\Omega},E) \\ & - \int_{4\pi} d\boldsymbol{\Omega}' \int dE' \Sigma_s(\boldsymbol{r},\boldsymbol{\Omega}'\to\boldsymbol{\Omega},E'\to E)\phi(\boldsymbol{r},\boldsymbol{\Omega}',E'),\end{aligned} \tag{2}$$

$\phi(\boldsymbol{r},\boldsymbol{\Omega},E)$ is the flux at position $\boldsymbol{r}$ with energy E and direction $\boldsymbol{\Omega}$, $\chi(E)$ the fission neutron spectrum, $S(\boldsymbol{r})$ the fission source at position $\boldsymbol{r}$ inherited from the previous generation, Σ_t the total cross section, and Σ_s the scattering cross section. After obtaining $\phi(\boldsymbol{r},\boldsymbol{\Omega},E)$ through the random walk process in one generation, the *k*-eigenvalue of the generation is expressed as

$$k_{eff} = \frac{\langle \nu\Sigma_f(\boldsymbol{r},E)\phi(\boldsymbol{r},\boldsymbol{\Omega},E)\rangle}{\langle S(\boldsymbol{r})\rangle}, \tag{3}$$

where ν is the number of neutrons per fission, Σ_f is the fission cross section, and the angle brackets denote integration over the entire phase space. The fission source used in the next generation is expressed as

$$S(\boldsymbol{r}) = \frac{1}{k_{eff}} \int d\boldsymbol{\Omega} \int dE\, \nu\Sigma_f(\boldsymbol{r},E)\phi(\boldsymbol{r},\boldsymbol{\Omega},E), \tag{4}$$

where k_{eff} is introduced to retain an almost constant number of fission neutrons over the generations.

First, we discuss the PSM under the condition that the fission source is unchanged by the perturbation of the cross sections. Suppose that the cross sections (including the fission neutron spectrum) in Eq. (2) are changed to $\Sigma_t + \Delta\Sigma_t$, $\Sigma_s + \Delta\Sigma_s$, and χ^p, respectively. Therefore, Eq. (1) in the perturbed system changes to

$$(\boldsymbol{H} + \Delta\boldsymbol{H})\big(\phi(\boldsymbol{r},\boldsymbol{\Omega},E) + \delta\phi^{NP}(\boldsymbol{r},\boldsymbol{\Omega},E)\big) = \frac{\chi^p(E)}{4\pi} S(\boldsymbol{r}), \tag{5}$$

where

$$\Delta\boldsymbol{H}(\cdots) \equiv \Delta\Sigma_t(\boldsymbol{r},E)(\cdots) - \int_{4\pi} d\boldsymbol{\Omega}' \int dE' \Delta\Sigma_s\big(\boldsymbol{r},\boldsymbol{\Omega}'\to\boldsymbol{\Omega},E'\to E\big)(\cdots), \tag{6}$$

Here, $\delta\phi^{NP}$ is the flux change caused by the perturbation of the cross sections, $\chi^p(E)$ is the perturbed fission neutron spectrum, and the superscript *NP* denotes that the effect of fission source perturbation is not included. The transport equation for $\delta\phi^{NP}$ is obtained by subtracting Eq. (1) from Eq. (5) as follows:

$$(\boldsymbol{H} + \Delta\boldsymbol{H})\delta\phi^{NP}(\boldsymbol{r},\boldsymbol{\Omega},E) = -\Delta\boldsymbol{H}\phi(\boldsymbol{r},\boldsymbol{\Omega},E) + \frac{\chi^p(E) - \chi(E)}{4\pi} S(\boldsymbol{r}). \tag{7}$$

The first term on the right-hand side of Eq. (7) represents one of the source terms and is written as

$$\begin{aligned} -\Delta\boldsymbol{H}\phi(\boldsymbol{r},\boldsymbol{\Omega},E) &= -\Delta\Sigma_t(\boldsymbol{r},E)\phi(\boldsymbol{r},\boldsymbol{\Omega},E) \\ &+ \int_{4\pi} d\boldsymbol{\Omega}' \int dE' \Delta\Sigma_s\big(\boldsymbol{r},\boldsymbol{\Omega}'\to\boldsymbol{\Omega},E'\to E\big)\phi\big(\boldsymbol{r},\boldsymbol{\Omega}',E'\big). \end{aligned} \tag{8}$$

If the neutron flux in the unperturbed system ϕ is known, then we can obtain the perturbed flux $\delta\phi^{NP}$ by solving the transport equation for $\delta\phi^{NP}$in Eq. (7). After $\delta\phi^{NP}$ is obtained, the *k*-eigenvalue change without fission source perturbation is expressed as

$$\Delta k_{eff}^{NP} = \frac{\langle (\nu\Sigma_f(\boldsymbol{r},E) + \delta(\nu\Sigma_f(\boldsymbol{r},E)))\delta\phi^{NP}(\boldsymbol{r},\boldsymbol{\Omega},E)\rangle}{\langle S(\boldsymbol{r})\rangle} + \frac{\langle \delta(\nu\Sigma_f(\boldsymbol{r},E))\phi(\boldsymbol{r},\boldsymbol{\Omega},E)\rangle}{\langle S(\boldsymbol{r})\rangle}, \quad (9)$$

where $\delta(\nu\Sigma_f)$ is the change in $\nu\Sigma_f$. The Monte Carlo algorithm used in the PSM to solve fixed-source problems that is presented in [20, 21] can be used to calculate Δk_{eff}^{NP}.

2.2 Perturbation source method with fission source perturbation

The formulation in Section 2.1 does not include the perturbed source effect. In this section, the PSM that considers the perturbed source effect is presented.

At a position $\boldsymbol{r}$, the fission source perturbed by cross-section changes is expressed as

$$\delta S(\boldsymbol{r}) = \delta S_1(\boldsymbol{r}) + \delta S_2(\boldsymbol{r}), \quad (10)$$

where

$$\delta S_1(\boldsymbol{r}) = \int d\boldsymbol{\Omega} \int dE\, \delta(\nu\Sigma_f(\boldsymbol{r},E))\phi(\boldsymbol{r},\boldsymbol{\Omega},E)\,, \quad (11)$$

and

$$\delta S_2(\boldsymbol{r}) = \int d\boldsymbol{\Omega} \int dE\, (\nu\Sigma_f(\boldsymbol{r},E) + \delta(\nu\Sigma_f(\boldsymbol{r},E)))\delta\phi_p(\boldsymbol{r},\boldsymbol{\Omega},E)\,. \quad (12)$$

Eq. (11) represents the perturbation caused by an unperturbed flux and the change in $\nu\Sigma_f$. Eq. (12) represents the perturbation caused by a flux change and the perturbed $\nu\Sigma_f$. The $\delta\phi_p$ term in Eq. (12) is defined in Eq. (14) below. The perturbed fission source must be normalized with respect to the unperturbed fission source as follows:

$$S_p(\boldsymbol{r}) = (S(\boldsymbol{r}) + \delta S(\boldsymbol{r}))\frac{\langle S(\boldsymbol{r})\rangle}{\langle S(\boldsymbol{r}) + \delta S(\boldsymbol{r})\rangle}, \quad (13)$$

where $\langle S(\boldsymbol{r})\rangle$ is the same as that in Eq. (4). The equation for the k-eigenvalue in the perturbed system, which includes the perturbed source effect, is written as

$$(\boldsymbol{H} + \Delta\boldsymbol{H})\big(\phi(\boldsymbol{r},\boldsymbol{\Omega},E) + \delta\phi_p(\boldsymbol{r},\boldsymbol{\Omega},E)\big) = \frac{\chi^p(E)}{4\pi}S_p(\boldsymbol{r}), \quad (14)$$

where $\delta\phi_p$ is the perturbed flux due to cross-section changes and fission source perturbation. Subtracting Eq. (5) from Eq. (14) yields

$$(\boldsymbol{H} + \Delta\boldsymbol{H})\delta\phi^{PS}(\boldsymbol{r},\boldsymbol{\Omega},E) = \frac{\chi^p(E)}{4\pi}(S_p(\boldsymbol{r}) - S(\boldsymbol{r})), \quad (15)$$

where $\delta\phi^{PS}$ is the difference in flux difference due to fission source perturbation and is expressed as

$$\delta\phi^{PS}(\boldsymbol{r},\boldsymbol{\Omega},E) \equiv \delta\phi_p(\boldsymbol{r},\boldsymbol{\Omega},E) - \delta\phi^{NP}(\boldsymbol{r},\boldsymbol{\Omega},E). \quad (16)$$

Using $\delta\phi^{PS}$, the *k*-eigenvalue change caused by fission source perturbation is expressed as

$$\Delta k_{eff}^{PS} = \frac{\left\langle (\nu\Sigma_f(\boldsymbol{r},E) + \delta(\nu\Sigma_f(\boldsymbol{r},E)))\delta\phi^{PS}(\boldsymbol{r},\boldsymbol{\Omega},E)\right\rangle}{\langle S(\boldsymbol{r})\rangle}. \quad (17)$$

Consequently, the exact change in the *k*-eigenvalue arising from cross-section changes is expressed as the sum of the *k*-eigenvalue changes with and without the effect of fission source perturbation, as follows:

$$\Delta k_{eff} = \Delta k_{eff}^{NP} + \Delta k_{eff}^{PS}. \quad (18)$$

3. Monte Carlo algorithm of perturbation source method for *k*-eigenvalue problems

3.1. Calculation flow

This section presents a Monte Carlo algorithm for implementing the formulation described in Section 2. The Monte Carlo algorithm for Δk_{eff}^{NP} is similar to that for the fixed-source calculations presented in [20, 21]. We begin with a situation where the fission source distribution has already attained its convergence after a sufficient number of inactive generations, and the fundamental mode flux $\phi(\boldsymbol{r},\boldsymbol{\Omega},E)$ is known. The PSM without the perturbed fission source effect for one generation calculation is performed as follows, and the schematic flow diagram is shown in **Figures 1(a)** and **1(b)**.

(1) The calculation is composed of two calculation modes. One is the unperturbed calculation mode, where a conventional *k*-eigenvalue calculation is performed for the *unperturbed* system; Eq. (1) is used for this mode. The other is the perturbation calculation mode that is performed for the perturbed system; Eq. (7) is used for this mode.

(2) First, a particle is started from a fission source site that is sampled from the fission source distribution $S(\boldsymbol{r})$ in Eq. (5). Before starting the unperturbed calculation mode, the fission spectrum change is calculated. At the beginning of each particle history, a "perturbation

particle" that corresponds to the second term on the right-hand side of Eq. (7) is emitted with the energy sampled from the *unperturbed* fission spectrum. The weight of the perturbation particle is expressed as

$$W_{sp} = \frac{\chi^p(E) - \chi(E)}{\chi(E)} W, \tag{19}$$

where W is the weight of the fission source and is typically almost unity. As illustrated in **Figure 1(b)**, the random walk process is performed for this perturbation particle in the *perturbed* system until it is killed by leakage or the Russian roulette game.

(3) After the perturbation particle in step (2) is killed, a perturbation particle that represents the fission source perturbation is emitted from the same fission source site in the same manner as in step (2). This perturbation particle corresponds to the right-hand side of Eq. (15) $S_p(\boldsymbol{r}) - S(\boldsymbol{r})$, and it has a weight of W_{ps}. The method to determine W_{ps} is discussed below. The energy of the particle is sampled from the *perturbed* fission spectrum $\chi^p(E)$. This perturbation particle is tracked in the *perturbed* system until it is killed.

(4) After steps (2) and (3) are completed, the mode is switched to the unperturbed calculation mode. This mode is identical to those of ordinary *k*-eigenvalue calculations. The same particle that is used in step (2) is used again, but the weight is W instead of W_{sp}. This particle is tracked in an *unperturbed* system.

(5) Each time the particle in step (4) undergoes collision in a perturbed region where the cross sections are changed from those in the unperturbed system, the random walk process is suspended. Subsequently, the calculation mode is switched to the perturbation calculation mode, where the random walk process for Eq. (7) is performed. In this perturbation calculation mode, two perturbation particles are started separately from the collision site.

(5.1) The first term, which is due to the change in the total cross section, corresponds to the first term on the right-hand side of Eq. (8). The weight of the first perturbation particle is expressed as

$$W_t = -(\Sigma_t^p - \Sigma_t^{un})\frac{W}{\Sigma_t^{un}}, \quad (20)$$

where W is the weight before collision in the unperturbed calculation mode; Σ_t^p and Σ_t^{un} are the perturbed and unperturbed total cross sections, respectively. The energy and direction of this perturbation particle are unchanged from those of the particle before collision. The random walk process is performed for this perturbation particle in the *perturbed* system until it is killed.

(5.2) The second perturbation particle, which is due to the change in the scattering cross section, corresponds to the second term on the right-hand side of Eq. (8). The weight of the second perturbation particle is expressed as

$$W_{sc} = \left(\frac{f^p(\boldsymbol{\Omega}\cdot\boldsymbol{\Omega}', E\to E')}{f^{un}(\boldsymbol{\Omega}\cdot\boldsymbol{\Omega}', E\to E')}\Sigma_s^p - \Sigma_s^{un}\right)\frac{W}{\Sigma_t^{un}}, \quad (21)$$

where Σ_s^p and Σ_s^{un} are the perturbed and unperturbed total scattering cross sections, respectively, and $f(\boldsymbol{\Omega}\cdot\boldsymbol{\Omega}', E\to E')$ is the probability density at which the direction and energy after scattering become $\boldsymbol{\Omega}'$ and E' from $\boldsymbol{\Omega}$ and E, respectively. The superscript p or un on f denotes that the scattering law belongs to the perturbed or unperturbed system, respectively. After the first perturbation particle in step (5.1) is killed, the second perturbation particle is emitted in direction $\boldsymbol{\Omega}'$ and energy E' sampled from the scattering law in the *unperturbed* system. Subsequently, the random walk process is performed for this second perturbation particle in the *perturbed* system until it is killed. In [4], two perturbation particles that correspond to Σ_s^p and Σ_s^{un}, separately, are emitted independently. This study improves this algorithm by consolidating two perturbation particles into one particle, as defined in Eq. (21). This algorithm can be straightforwardly implemented in multi-group problems. The possibility of applying the method proposed in this study to continuous energy Monte Carlo codes depends on whether Eq. (21) can be determined in the codes. Even if it cannot be determined, this difficulty can be circumvented by choosing an algorithm where two

perturbation particles are emitted as proposed in [4] at the expense of adding another perturbation particle.

(6) After steps (5.1) and (5.2) are completed, the mode returns to the unperturbed calculation mode. The random walk that is suspended at step (5) is resumed and continues until the end of the history, similar to ordinary *k*-eigenvalue calculations.

(7) The numerator of the second term on the right-hand side of Eq. (9) is obtained by accumulating the following estimates for each collision during the random walks in step (6):

$$\langle \delta(\nu\Sigma_f(\boldsymbol{r},E))\phi(\boldsymbol{r},\boldsymbol{\Omega},E)\rangle = F_{NP,1} \equiv \sum_i (\delta(\nu\Sigma_f))\frac{W_i}{\Sigma_t}, \tag{22}$$

where the summation is performed over all collisions during history, and *i* denotes the *i*th collision.

(8) The numerator of the first term on the right-hand side of Eq. (9) is obtained by accumulating the following estimates for each collision during the random walks in steps (2), (5.1), and (5.2):

$$\langle (\nu\Sigma_f(\boldsymbol{r},E) + \delta(\nu\Sigma_f(\boldsymbol{r},E)))\delta\phi^{NP}(\boldsymbol{r},\boldsymbol{\Omega},E)\rangle = F_{NP,2} \equiv$$

$$= \sum_i (\nu\Sigma_f)_p \frac{W_{sp,i}}{\Sigma_t} + \sum_i (\nu\Sigma_f)_p \frac{W_{t,i}}{\Sigma_t} + \sum_i (\nu\Sigma_f)_p \frac{W_{sc,i}}{\Sigma_t}, \tag{23}$$

where $(\nu\Sigma_f)_p$ is $\nu\Sigma_f$ in the perturbed system; $W_{sp,i}$, $W_{t,i}$, and $W_{sc,i}$ are the weights at the *i*th collision in steps (2), (5.1), and (5.2), respectively.

(9) After steps (1)–(8) are completed for all fission sources in one generation, the calculation for the generation is terminated. The fission and perturbed fission sources calculated in this generation are succeeded to the next generation. The *k*-eigenvalue change without fission source perturbation is obtained at the end of the generation as follows:

$$\Delta k_{eff}^{NP} = \frac{1}{N}(F_{NP,1} + F_{NP,2}), \tag{24}$$

where N is the nominal number of source histories per generation; $F_{NP,1}$ and $F_{NP,2}$ are defined as shown in Eqs. (22) and (23), respectively.

3.2. Perturbation of fission source

As described in step (3) in Section 3.1, $S_p(\boldsymbol{r})$ and $S_p(\boldsymbol{r}) - S(\boldsymbol{r})$ must be obtained to calculate the fission source perturbation. Whereas $S(\boldsymbol{r})$ is produced during the ordinary *k*-eigenvalue calculation in the unperturbed system, $S_p(\boldsymbol{r})$ is produced by the unperturbed flux ϕ and the flux difference, $\delta\phi_p$ as shown in Eqs. (10)−(13). The fission sources $S(\boldsymbol{r})$ and $S_p(\boldsymbol{r})$ are not produced at the same point, thereby precluding the pointwise assignment of $S_p(\boldsymbol{r}) - S(\boldsymbol{r})$. Therefore, the region where fissions occur is spatially discretized into small bins, as adopted in [4]. The fission sources produced by ϕ or $\delta\phi_p$ are stored in each bin every time a collision occurs. During the random walks, the following fission source is accumulated in the *k*th bin to calculate $\delta S(\boldsymbol{r})$ defined in Eq. (10):

$$\delta S_k = \sum_i (\delta(\nu\Sigma_f))\frac{W_{i,k}}{\Sigma_t} + \sum_i (\nu\Sigma_f)_p \frac{W_{sp,i,k}}{\Sigma_t} + \sum_i (\nu\Sigma_f)_p \frac{W_{t,i,k}}{\Sigma_t} + \sum_i (\nu\Sigma_f)_p \frac{W_{sc,i,k}}{\Sigma_t} + \sum_i (\nu\Sigma_f)_p \frac{W_{ps,i,k}}{\Sigma_t}, \quad (25)$$

where $W_{i,k}$, for example, denotes the weight at the *i*th collision in the *k*th bin. The first four terms on the right-hand side of Eq. (25) are defined in Eqs. (22) and (23): The last term on the right-hand side is obtained by accumulating the estimates at each collision during the random walks in step (3), and $W_{ps,i,k}$ is the weight used in step (3). The last four terms are calculated by the additional random walks in the *perturbed* system, i.e., four perturbation calculation modes are invoked in the newly proposed PSM. Similarly, the fission source in the unperturbed system $S(\boldsymbol{r})$ is accumulated in each bin as follows:

$$S_k = \sum_i \nu\Sigma_f \frac{W_{i,k}}{\Sigma_t}. \quad (26)$$

After all particle histories for one generation are completed, the number of fission sources in the *k*th bin to be used in the next generation is calculated as follows:

$$n_k = \mathrm{Int}[S_k + \xi], \quad (27)$$

where Int[x] denotes the largest integer not exceeding x, and ξ is a pseudo-random number between 0 and 1. Before proceeding to the next generation, S_k and $T_k \equiv (S_k + \delta S_k)$ are normalized with respect to N as follows:

$$S'_k = S_k \frac{N}{\sum_k S_k}, \tag{28}$$

$$T'_k = (S_k + \delta S_k) \frac{N}{\sum_k (S_k + \delta S_k)}, \tag{29}$$

where N is the nominal number of source histories per generation, and the summation is performed over all bins. The weight of the starting particles in step (3), $W_{ps,k}$, to be assigned to the particles in the kth bin is calculated as follows:

$$W_{ps,k} = \frac{T'_k}{S'_k} - 1, \tag{30}$$

which corresponds to the source term $S_p(\boldsymbol{r}) - S(\boldsymbol{r})$ in the transport equation for $\delta\phi^{PS}$ in Eq. (15). According to Eq. (15), the random walk process is performed using this perturbation particle in the *perturbed* system for step (3) until it is killed. At the end of the generation, the k-eigenvalue change due to fission source perturbation is obtained as follows:

$$\Delta k_{eff}^{PS} = \frac{1}{N} \sum_i (\nu\Sigma_f)_p \frac{W_{ps,i}}{\Sigma_t}. \tag{31}$$

Based on Eqs. (25), (29), and (30), the weight for the fission source perturbation, W_{ps}, must be obtained recursively. Hence, this weight is iteratively updated in each generation, and the convergence of Δk_{eff}^{PS} must be assessed before active generations are started.

The weights that begin from the fission sources are set to $N/M(\approx 1)$, $W_{sp}N/M$, and $W_{ps}N/M$ in steps (1), (2), and (3), respectively, where M is the sum of n_k in Eq. (27). These starting particles are distributed uniformly within each bin where they are produced.

In the conventional Monte Carlo perturbation methods (e.g., iterated fission probability, differential operator sampling, CS), the memory required may become extremely large because the information of fission sources must be retained during latent

generations (≈ 10). Meanwhile, in the PSM, the information for fission source perturbation are stored for only one generation, thereby alleviating large memory requirement.

3.3. Improvement in efficiency

Perturbation particles are not emitted until a particle undergoes collision in a perturbed region. If the perturbed region occupies only a small fraction of the entire system or the density is extremely low, then collisions will seldom occur in the perturbed region, thereby reducing the number of perturbation particles emitted and rendering the calculation less efficient. The pseudo-scattering method proposed in [20, 21] aims to increase the number of perturbation particles. In this method, a pseudo-scattering cross section is added to the cross section in the perturbed region by multiplying the total cross section Σ_t by a factor of C (>1), as follows:

$$\Sigma_t^* = C \cdot \Sigma_t . \tag{32}$$

The random walk process for the unperturbed calculation mode is performed using this pseudo total cross section. At every collision point in the perturbed region, a perturbation particle is started with a weight W_t/C or, W_{sc}/C where W_t and W_{sc} are defined in Eqs. (20) and (21), respectively: The division of the weight by C is introduced to compensate for the increased pseudo total cross section. After the perturbation particle is killed in the perturbation calculation mode, the suspended unperturbed calculation mode is resumed. Before resuming the unperturbed calculation mode, whether the pseudo collision is accepted as a real collision is determined based on the following criterion:

$$\xi < \frac{\Sigma_t}{\Sigma_t^*} = \frac{1}{C}, \tag{33}$$

where ξ is a pseudo-random number between 0 and 1. If the criterion is rejected, then the particle maintains its direction, energy, and weight before the pseudo collision, and it continues flying. If the criterion is satisfied, then the collision is treated as a real one. As the factor C increases, the number of collisions increases in the perturbed region, thereby increasing the number of perturbation particles emitted. As demonstrated in [20, 21], the

pseudo-scattering method improves the computation efficiency, particularly when the perturbed region is small.

4. Numerical examples

4.1 Verification (Cases 1 and 2)

Numerical tests were performed to verify the algorithm for calculating a *k*-eigenvalue change, as described in Section 3. Throughout this study, the geometries of the numerical examples were two-dimensional rectangles, and three-energy group constants were used. A vacuum boundary condition was imposed on the external boundaries. In the first test problem, a large *k*-eigenvalue change was induced to verify the new method. The central region of a homogeneous material was perturbed, as shown in **Figure 2**. The dimensions shown in **Figure 2** are $a = 24$ cm and $b = 4$ cm. The three-group constants used in this section are listed in Tables 1 and 2. Throughout this study, the scatterings were isotropic. In this problem, material (1) is identical to material (2) in **Figure 2**. For all cases investigated in this study, 100,000 histories were used per generation, and the initial 20 generations were discarded. The number of total generations varied depending on the property of the problem. The reference solution was obtained by the difference in *k*-eigenvalues between two independent Monte Carlo calculations before and after the perturbation, which is referred to the "direct method" hereinafter. Another reference solution was obtained using the discrete ordinates transport code DANTSYS [27] using the same group constants. To compare the PSM with another conventional Monte Carlo perturbation method, CS was applied to the problems in this study. The CS method used in this study, which can account for the effect of fission source perturbation, is based on the algorithm proposed in [1, 12]. The entire region was partitioned into 3 × 3 subregions and the subregions were divided into (300 + 100 + 300) × (300 + 100 +300) spatial bins to accumulate the fission sources. The *k*-eigenvalue changes calculated using the four methods (the PSM, CS, direct method, and deterministic method) are listed in Table 3. All statistical uncertainties in this study were one standard

deviation. The result of the PSM calculation was obtained using $C = 1$. Because the fission source perturbation effect Δk_{eff}^{PS} exceeded Δk_{eff}^{NP}, it was extremely challenging to verify the fission source perturbation effect numerically. However, the PSM calculation precisely reproduced the reference results. Meanwhile, the accuracy of Δk_{eff}^{PS} calculated by CS was unsatisfactory, indicating that the large perturbation in this problem is beyond of the applicability of CS. Table 4 shows a comparison of the relative figure-of-merit (FOM), which is expressed as

$$FOM = \frac{1}{\sigma^2 T}, \tag{34}$$

where σ is the one standard deviation of the absolute uncertainty, and T the computation time. The Monte Carlo perturbation methods (PSM and CS) are significantly less efficient than the direct method. The perturbation in this example is relatively large in terms of the cross-section change and perturbed region fraction, and the direct method can yield statistically precise results with shorter computation time. The number of perturbation particles emitted from the perturbed region increases with the perturbed region fraction, rendering the PSM less efficient. In such a case, increasing the factor C results in the deteriorated efficiency of the PSM, as shown in Table 4.

The convergence of Δk_{eff}^{NP} and Δk_{eff}^{PS} with respect to the generations are shown in **Figure 3**. Despite the large fission source perturbation effect, Δk_{eff}^{PS} converged before the 20th generation, and the discarded inactive generations (20) were considered to be sufficient.

In Case 1, an extremely large perturbation was used to perform a precise verification of the PSM. The next example (Case 2) addresses a more moderate perturbation. The cross sections in the perturbed region are listed in Table 5. The other calculation conditions are identical to those in Case 1. The *k*-eigenvalue changes and the relative FOMs in Case 2 are listed in Tables 6 and 4, respectively. Both Monte Carlo perturbation methods (PSM and CS) outperformed the direct method. In general, CS is superior to the PSM for a small perturbation that extends over a relatively large region. Meanwhile, the PSM is superior for

a large perturbation that is added in a small region, as demonstrated below through some numerical examples.

The calculation results may depend on the spatial bin sizes for calculating the fission source perturbation effect. The dependence of the calculation results on the mesh spacing is discussed in Appendix.

4.2 Perturbation in small region (Cases 3 and 4)

In the next test problem (Case 3), a central region in a homogenized light-water-moderated UO_2 fuel rod array is replaced with light water. The dimensions shown in **Figure 2** are a = 35 cm and b = 1.32 cm. The entire region was partitioned into 3 × 3 subregions and the subregions were divided into (130 + 20 + 130) × (130 + 20 +130) spatial bins. Tables 7 and 8 show the three-energy group constants for the two materials. The group constants were prepared using the standard reactor analysis code (SRAC) [28]. The k-eigenvalue changes and relative FOMs in Case 3 are listed in Tables 9 and 4, respectively. The result of the PSM agreed well with that of the deterministic method. The significant difference between the PSM and direct method was due to the large statistical uncertainty in the direct method. The results of CS differed from those of other methods. For a large perturbation such as that in this problem, where a material is replaced with another one, CS can no longer yield reliable results. As shown in Table 4, increasing the factor C improves the efficiency of the PSM. The FOM is maximized at $C \sim 5$.

In the next test problem (Case 4), a perturbation is added to the central region (1.32 cm × 1.32 cm) of the perturbed system in Case 3. The light water density in the central region decreased by 10%. The k-eigenvalue changes and relative FOMs in Case 4 are listed in Tables 10 and 4, respectively. The PSM exhibited excellent performance for this problem. Although CS does not perform as well as the PSM, CS is applicable to this problem. The efficiency of the PSM is further improved by adjusting the factor C. The maximized FOM, which is four times the FOM with C = 1, was attained at $C \sim 20$.

4.3 Interface displacement (Cases 5 and 6)

This section presents a perturbation where the interface between two regions is displaced. In this test problem, a graphite reflector with a thickness of 10 cm was attached to the homogeneous UO_2 fuel rod array, as shown in **Figure 4**. In the first example, in Case 5, the interface between the graphite and UO_2 fuel regions is displaced to the right by 1 cm. The interface displacement is equivalent to replacing the 1-cm-thick graphite adjacent to the interface with the UO_2 fuel region. The entire region was partitioned into 3 × 1 subregions and the subregions were divided into (700 + 70 + 50) × 700 spatial bins. Table 11 shows the three-energy group constants for graphite. The *k*-eigenvalue changes and relative FOMs in Case 5 are listed in Tables 12 and 13, respectively. Because CS yielded wrong results for this problem, the results of CS were omitted in the tables. The result of the PSM agreed well with those of the direct and deterministic methods. However, the efficiency of the PSM with respect to the direct method was mediocre because of the relatively large perturbed region (1 cm × 35 cm) in this problem.

In Case 6, the interface was displaced by 0.02 cm, which was much smaller than in Case 5. The *k*-eigenvalue changes and relative FOMs in Case 6 are listed in Tables 14 and 13, respectively. Whereas the *k*-eigenvalue change by the direct method was not statistically significant, the PSM yielded a result that agreed well with the reference value by the deterministic method. The efficiency of the PSM was maximized at $C \sim 40$, the effect of which was enhanced by a factor of six compared with the case of $C = 1$.

4.4 External boundary extension (Cases 7 and 8)

In the last two numerical examples, Cases 7 and 8, the external right boundary of the graphite reflector extended by 3 cm and 0.02 cm, respectively, as shown in **Figure 5**. This perturbation is equivalent to replacing the void region adjacent to the right end of the graphite in the unperturbed system with the extended graphite. However, CS and PSM cannot manage such perturbations, where a void region is replaced with a nonvoid material because particles

that leave an external boundary do not contribute to the subsequent perturbation calculations. Some methods to circumvent this limitation have been proposed [21]. The simple method adopted in this study was by displacing the extended boundary to the unperturbed location instead of extending the external boundary. The entire region was partitioned into 3 × 1 subregions and the subregions were divided into (700 + 50 + 50) × 700 spatial bins. The *k*-eigenvalue change caused by the boundary extension was obtained by reversing the sign of the result. Using this method, the *k*-eigenvalue changes caused by the external boundary displacement by 3 and 0.02 cm were calculated, and the results are listed in Tables 15 and 16, respectively. The relative FOMs of the results are listed in Table 13. In Table 16 (Case 8), the result of the direct method is omitted because it is not statistically significant owing to its small value. In both cases, the PSM and CS yielded satisfactory results compared with the deterministic method. For the relatively large boundary displacement in Case 7, CS exhibited an efficient performance comparable to that of the PSM. Meanwhile, for the small boundary extension in Case 8, the efficiency of the PSM was improved by increasing the factor *C* up to 3500.

5. Conclusion

The PSM, which can be applied to perturbation calculations in the *k*-eigenvalue mode, was revisited in this study. It was confirmed that the PSM can yield an accurate *k*-eigenvalue change caused by cross-section changes for various types of perturbations. The effect of fission source perturbation, which is the most formidable problem in *k*-eigenvalue problems, was successfully implemented via spatial discretization, as proposed by Hoffman et al. The method is almost exact except that it incurs an approximation in the spatial discretization for fission source perturbation. CS, which is another exact Monte Carlo method, has a weakness for large cross-section changes such as the replacement of a material with another one. The PSM is a robust method for large perturbations that cannot be addressed by CS owing to its unbounded statistical uncertainty. A larger perturbed region

signifies that more perturbation particles emitted from the perturbed region need to be tracked, which worsens the efficiency of the PSM for perturbations in a larger perturbed region. Meanwhile, the PSM exhibited excellent efficiency for perturbations added in a small region. The pseudo-scattering method, which was proposed by the authors for fixed-source problems, was applied in this study to improve computation efficiency. The efficiency can be further improved by adjusting a factor for the pseudo-scattering method. The algorithm for fission source perturbation in the PSM can reduce the large memory requirements of conventional Monte Carlo perturbation methods. Although the propose method was verified for the multi-group problems, this can be applied to continuous energy Monte Carlo codes with slight modification.

Future work includes developing a new algorithm that does not require spatial discretization for fission source perturbation such that the PSM becomes applicable to more general problems.

Appendix

The effect of the spatial bin size on *k*-eigenvalue changes was studied for Case 2. The *k*-eigenvalue changes that were calculated with several spatial bin sizes are listed in Table 17. Although the results were significantly affected by the number of the spatial bins, it was found that the effect was not so remarkable even for the considerably rough discretization such as (7 + 3 +7) × (7 + 3 + 7).

Disclosure statement

The authors report no potential conflict of interest.

References

[1] Kiedrowski BC. Review of early 21st-century Monte Carlo perturbation and sensitivity techniques for k-eigenvalue radiation transport calculations. Nucl Sci Eng. 2017;185:426−444.

[2] Takahashi H. Monte Carlo method for geometrical perturbation and its application to the pulsed fast reactor. Nucl Sci Eng. 1970;41;259–279.

[3] Matthes W. Calculation of reactivity perturbations with the Monte Carlo method. Nucl Sci Eng. 1972;47;234–237.

[4] Hoffman TJ, Petrie LM, Landers NF. A Monte Carlo perturbation source method for reactivity calculations. Nucl Sci Eng. 1978;66;60−66.

[5] Nakagawa M, Asaoka T. Improvement of correlated sampling Monte Carlo methods for reactivity calculations. J Nucl Sci Technol. 1978;15;400−410.

[6] Preeg WE, Tsang JSK. Comparison of correlated Monte Carlo techniques. Trans Am Nucl Soc. 1982;43;628–629.

[7] Rief H. Generalized Monte Carlo perturbation algorithms for correlated sampling and a second-order Taylor series approach. Ann Nucl Energy. 1984;9;455–476.

[8] Lux I, Koblinger L. Monte Carlo Particle Transport Methods: Neutron and Photon Calculations, CRC Press, Boca Raton, Florida, 1991.

[9] McKinney GW, Iverson JL. Verification of the Monte Carlo differential operator technique for MCNP, Los Alamos National Laboratory, LA-13098, 1996.

[10] Kitada T, Yamane A, Takeda T. Improvements of correlated sampling method in Monte Carlo perturbation theory, Proc Int Conf on the Physics of Reactors PHYSOR96, Mito, Ibaraki, Japan, Sep. 16-20, 1996, A-212–A-219, 1996.

[11] Favorite JA. An alternative implementation of the differential operator (Taylor series) perturbation method for Monte Carlo criticality problems. Nucl Sci Eng. 2002;142;327–341.

[12] Nagaya Y, Mori T. Impact of perturbed fission source on the effective multiplication factor in Monte Carlo perturbation calculations. J Nucl Sci Technol. 2005;42;428–441.

[13] Kiedrowski BC, Brown FB, Wilson PPH. Adjoint-weighted tallies for k-eigenvalue calculations with continuous-energy Monte Carlo. Nucl Sci Eng. 2011;168;226–241.

[14] Terranova N, Mancusi D, Zoia A. New perturbation and sensitivity capabilities in TRIPOLI-4®. Ann Nucl Energy. 2018;121;335-349.

[15] Kim SH, Yamanaka M, Pyeon CH. Improvement of fission source distribution by correlated sampling method in Monte Carlo perturbation calculations. J Nucl Sci Technol. 2018;55;945–954.

[16] Nauchi Y, Kameyama T. Development of calculation technique for iterated fission probability and reactor kinetic parameters using continuous-energy Monte Carlo method. J Nucl Sci Technol. 2010;47;977–990.

[17] Shim HJ, Kim CH. Adjoint sensitivity and uncertainty analyses in Monte Carlo forward calculations. J Nucl Sci Technol. 2011;48;1453–1461.

[18] Choi SH, Shim HJ. Memory-efficient calculations of adjoint-weighted tallies by the Monte Carlo Wielandt method. Ann Nucl Energy. 2016;96;287–294.

[19] Qiu Y, Shang X, Tang X, et al. Computing eigenvalue sensitivity coefficients to nuclear data by adjoint superhistory method and adjoint Wielandt method implemented in RMC code. Ann Nucl Energy. 2016;87;228–241.

[20] Sakamoto H, Yamamoto T. Improvement and performance evaluation of the perturbation source method for an exact Monte Carlo perturbation calculation in fixed source problems. J Compt Phys. 2017;345;245–259.

[21] Yamamoto T, Sakamoto H. Monte Carlo perturbation calculation for geometry change in fixed source problems with the perturbation source method. Prog Nucl Energy 2021;132;103611.

[22] Nagaya Y, Mori T. Estimation of sample reactivity worth with differential operator sampling method. Prog Nucl Sci Technol. 2011;2;842–850.

[23] Favorite JA, Parsons DK. Second-order cross terms in Monte Carlo differential operator perturbation estimates," Proc M&C 2001, Salt Lake City, Utah, September 2001.

[24] Bell GI, Glasstone S. Nuclear Reactor Theory, Van Norstrand Reinhold, New York, 1970.

[25] Truchet G. Continuous-energy adjoint flux and perturbation calculation using the iterated fission probability method in Monte Carlo code TRIPOLI-4 and underlying applications." Proc Joint Int Conf on Supercomputing in Nuclear Applications and Monte Carlo 2013 (SNA + MC 2013), Paris, France, October 2013.

[26] Truchet G, Leconte P, Palau JM, et al. Sodium void reactivity effect analysis using the newly developed exact perturbation theory in Monte-Carlo code TRIPOLI-4®. Proc PHYSOR 2014 - The Role of Reactor Physics toward a Sustainable Future, Kyoto, Japan, September 2014.

[27] Alcouffe RE, Baker RS, Brinkley FW, et al. DANTSYS: A diffusion accelerated neutral particle transport code system. LA-12969-M. 1995.

[28] Okumura K, Kugo T, Kaneno K, et al. SRAC2006: A comprehensive neutronics calculation code system. JAEA-Data/Code 2007-004. 2007.

Table captions

Figure captions

Figure 1(a). Flow chart of unperturbed calculation mode.

Figure 1(b). Flow chart of perturbation calculation mode.

Figure 2. Geometry for perturbation calculations in Cases 1 to 4.

Figure 3. Δk with and without source perturbation effect as a function of generation.

Figure 4. Interface shift in Case 5 (x = 1 cm) and Case 6 (x = 0.02 cm).

Figure 5. External boundary extension in Case 7 (x = 3 cm) and Case 8 (x = 0.02 cm).

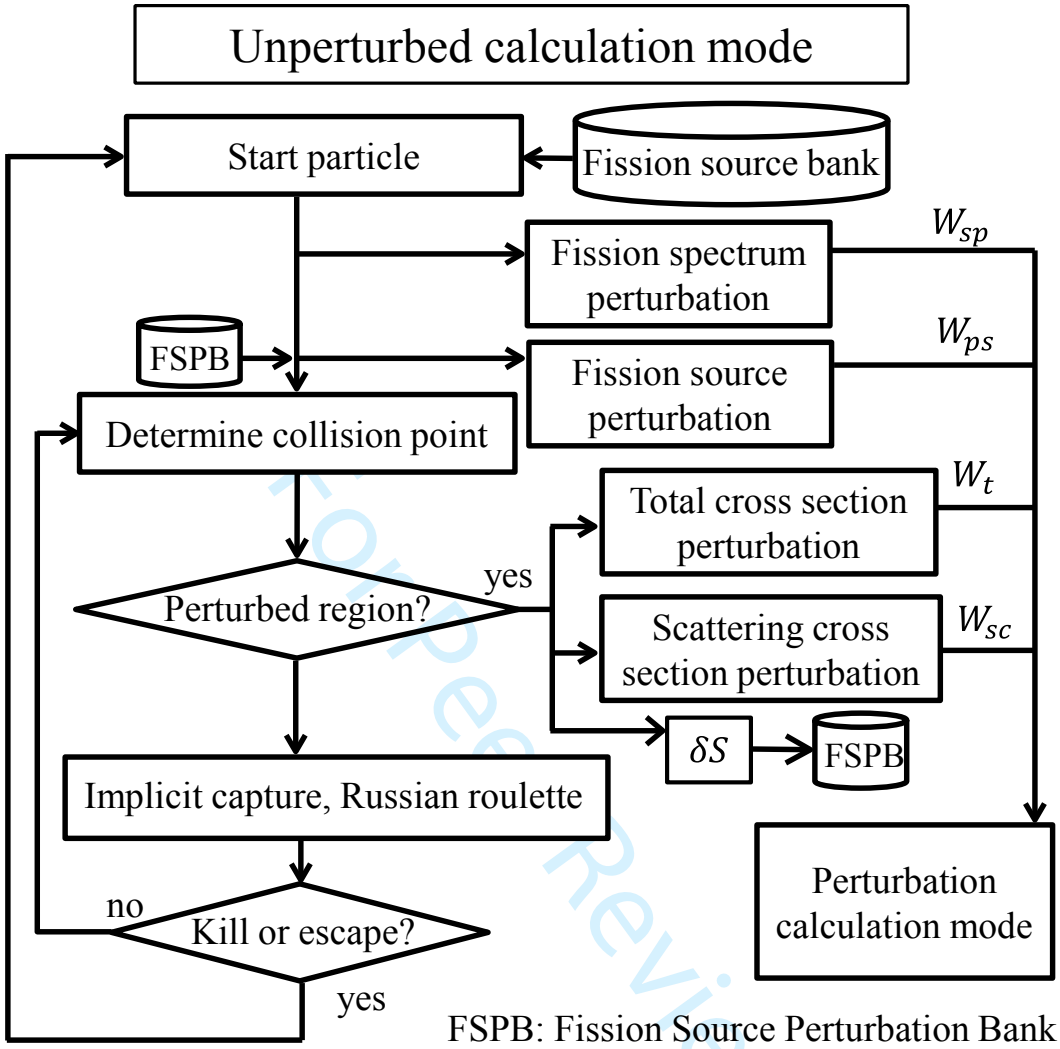

Figure 1(a). Flow chart of unperturbed calculation mode.

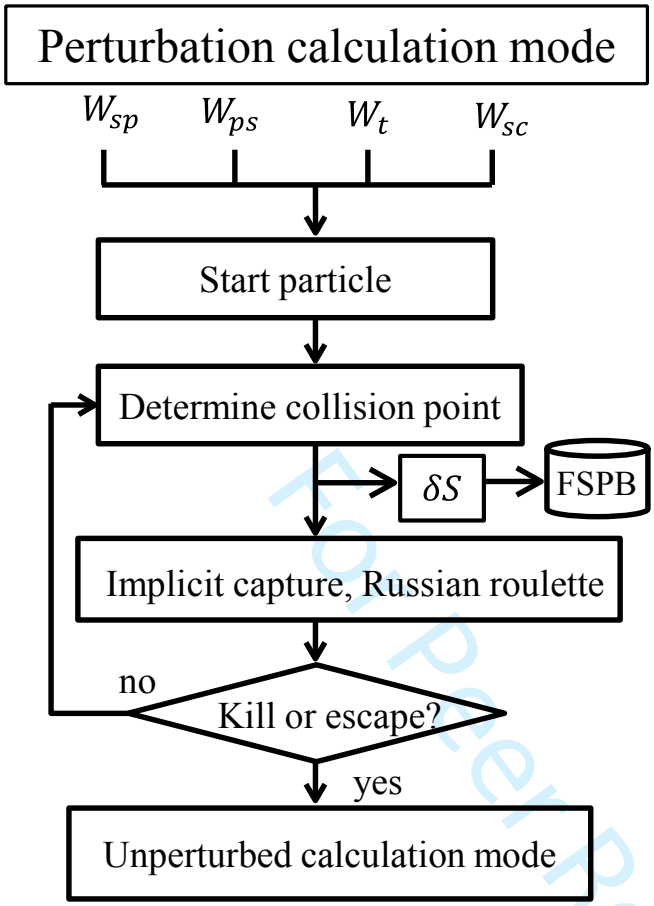

Figure 1(b). Flow chart of perturbation calculation mode.

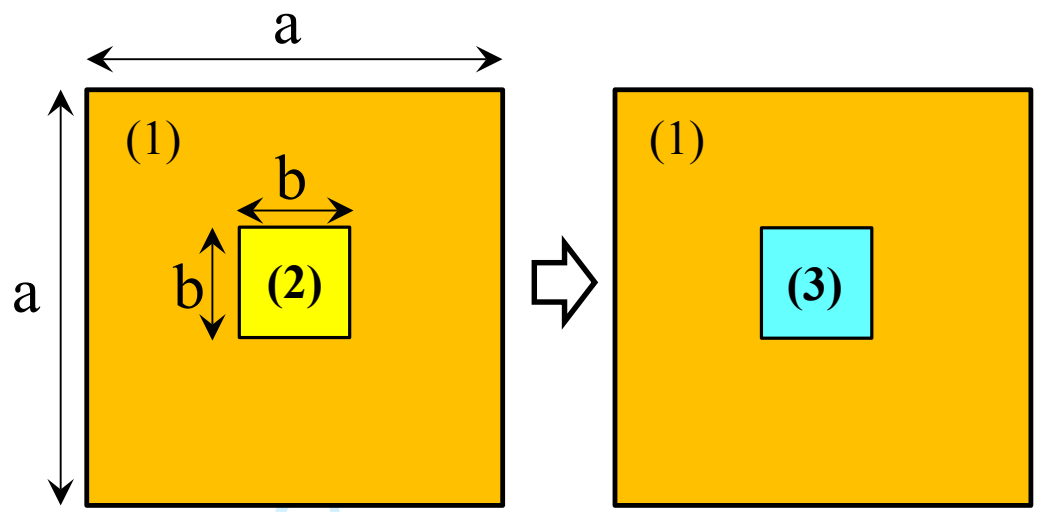

Figure 2. Geometry for perturbation calculations in Cases 1 to 4.

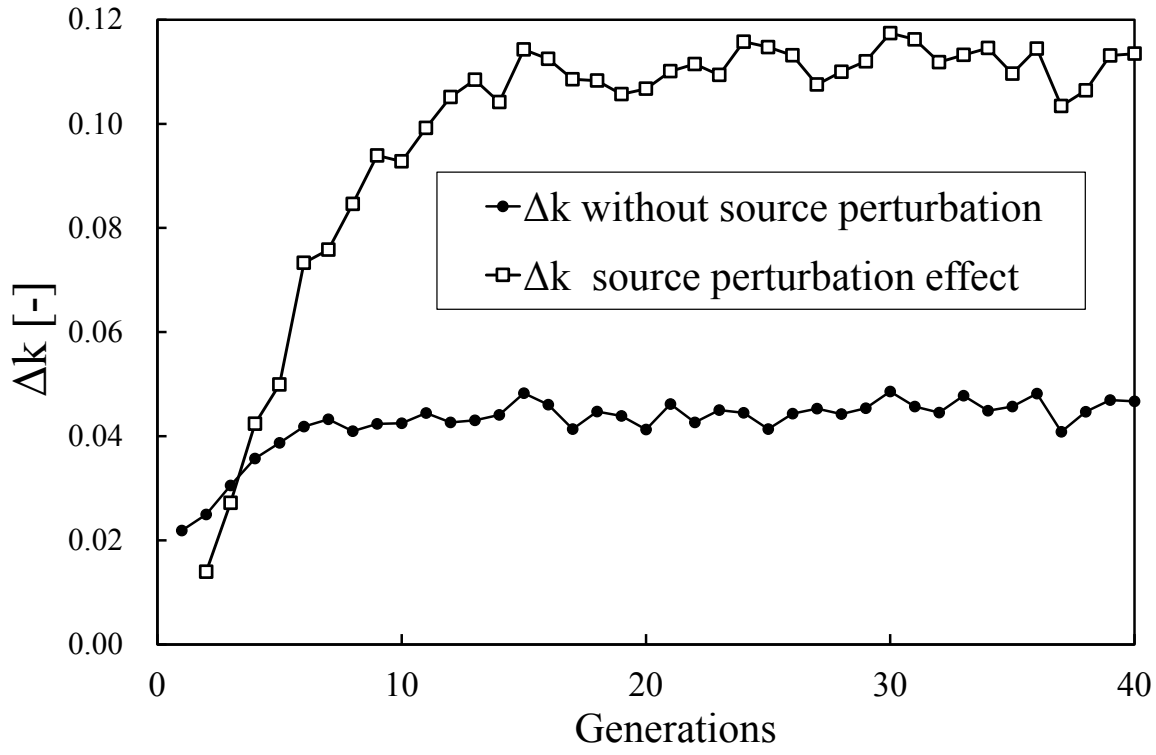

Figure 3. Δ*k* with and without source perturbation effect as a function of generation.

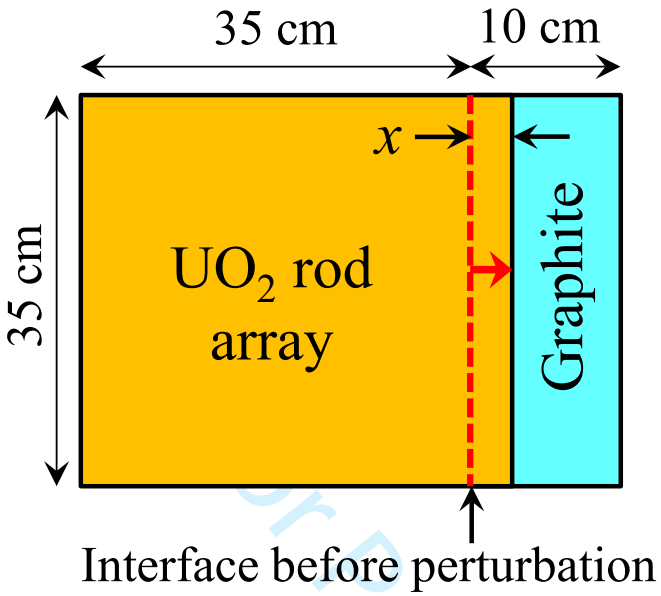

Figure 4. Interface shift in Case 5 (x = 1 cm) and Case 6 (x =0.02 cm).

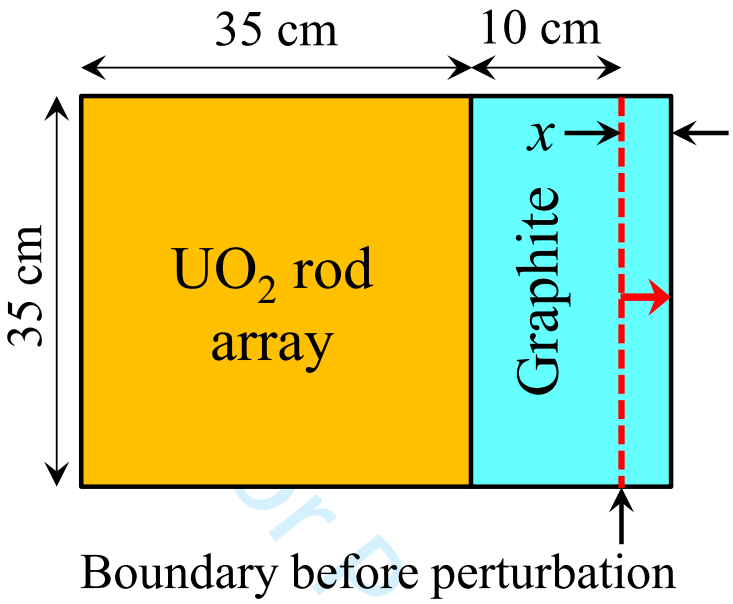

Figure 5. External boundary extension in Case 7 (x = 3 cm) and Case 8 (x = 0.02 cm).

Table 1. Three group constants of materials (1) and (2) in Figure 2 (Cases 1 and 2).

	1st group	2nd group	3rd group
$\Sigma_t\ (cm^{-1})$	1.0	1.5	3.0
$\Sigma_c(cm^{-1})$	0.01	0.02	0.03
$\Sigma_f(cm^{-1})$	0.01	0.04	0.06
ν	2.4	2.4	2.4
χ	0.8	0.2	0.0
$\Sigma_{sg\to g}(cm^{-1})$	0.882	1.296	2.91
$\Sigma_{sg\to g+1}(cm^{-1})$	0.098	0.144	0.0

Table 2. Three group constants of material (3) in Figure 2 (Case1).

	1st group	2nd group	3rd group
$\Sigma_t\ (cm^{-1})$	1.1	1.6	3.2
$\Sigma_c(cm^{-1})$	0.005	0.01	0.015
$\Sigma_f(cm^{-1})$	0.02	0.08	0.12
ν	2.4	2.4	2.4
χ	0.6	0.4	0.0
$\Sigma_{sg\to g}(cm^{-1})$	0.86	1.208	3.065
$\Sigma_{sg\to g+1}(cm^{-1})$	0.215	0.302	0.0

Table 3. *k*-eigenvalue changes for verification (Case 1).

	PSM (C=1)	CS
Δk_{eff}^{NP}	$4.4574\times10^{-2} \pm 5.9\times10^{-5}$	$4.4517\times10^{-2} \pm 2.4\times10^{-5}$
Δk_{eff}^{PS}	$1.1139\times10^{-1} \pm 1.2\times10^{-4}$	$9.9430\times10^{-2} \pm 9.4\times10^{-4}$
Total	$1.5596\times10^{-1} \pm 1.4\times10^{-4}$	$1.4395\times10^{-1} \pm 9.4\times10^{-4}$
Direct method	$1.5585\times10^{-1} \pm 4\times10^{-5}$	
Deterministic method	1.5586×10^{-1}	

Table 4. Relative figure-of-merit with respect to direct method. Number in parentheses denotes factor *C* in Eq. (32).

	Case 1	Case 2	Case 3	Case 4
Direct method	1	1	1	1
PSM	0.143 (C=1)	62.8 (C=1)	142 (C=1)	1092 (C=1)
	0.072 (C=2)	66.4 (C=2)	184 (C=5)	4377 (C=20)
	—	—	142 (C=10)	3701 (C=30)
CS	0.004	92.0	0.238	117

Table 5. Three group constants of material (3) in Figure 2 (Case2).

	1st group	2nd group	3rd group
$\Sigma_t\,(cm^{-1})$	1.05	1.52	3.05
$\Sigma_c(cm^{-1})$	0.009	0.018	0.029
$\Sigma_f(cm^{-1})$	0.011	0.045	0.065
ν	2.4	2.4	2.4
χ	0.78	0.22	0.0
$\Sigma_{sg\to g}(cm^{-1})$	0.9167	1.29673	2.956
$\Sigma_{sg\to g+1}(cm^{-1})$	0.1133	0.16027	0.0

Table 6. *k*-eigenvalue changes for verification (Case 2).

	PSM (C=1)	CS
Δk_{eff}^{NP}	$5.2507\times10^{-3} \pm 8.8\times10^{-6}$	$5.2342\times10^{-3} \pm 3.2\times10^{-6}$
Δk_{eff}^{PS}	$5.1664\times10^{-3} \pm 4.1\times10^{-6}$	$5.1028\times10^{-3} \pm 6.0\times10^{-6}$
Total	$1.0417\times10^{-2} \pm 9.6\times10^{-6}$	$1.0337\times10^{-2} \pm 6.8\times10^{-6}$
Direct method	$1.0366\times10^{-2} \pm 6.1\times10^{-5}$	
Deterministic method	1.0389×10^{-2}	

Table 7. Three group constants of UO_2 rod array (the materials (1) and (2) in Figure 2 (Case3)).

	1st group	2nd group	3rd group
$\Sigma_t\,(cm^{-1})$	0.29829	0.83334	1.6389
$\Sigma_c(cm^{-1})$	3.2674×10^{-3}	9.7371×10^{-3}	0.029252
$\Sigma_f(cm^{-1})$	3.0586×10^{-3}	2.1579×10^{-3}	0.056928
ν	2.4	2.4	2.4
χ	0.87820	0.12180	0.0
$\Sigma_{sg\to g}(cm^{-1})$	0.22106	0.77764	1.5527
$\Sigma_{sg\to g+1}(cm^{-1})$	0.073843	0.043803	0.0

Table 8. Three group constants of light water (the material (3) in Figure 2 (Case3)).

	1st group	2nd group	3rd group
$\Sigma_t\ (cm^{-1})$	0.33207	1.1265	2.7812
$\Sigma_c(cm^{-1})$	3.0500×10^{-4}	3.6990×10^{-4}	0.018250
$\Sigma_{sg\to g}(cm^{-1})$	0.22713	1.0281	2.7630
$\Sigma_{sg\to g+1}(cm^{-1})$	0.10464	0.097961	0.0

Table 9. *k*-eigenvalue changes for replacement of UO_2 with light water (Case 3).

	PSM (C=5)	CS
Δk_{eff}^{NP}	$9.1827\times10^{-5} \pm 2.52\times10^{-6}$	$1.4112\times10^{-4} \pm 4.64\times10^{-5}$
Δk_{eff}^{PS}	$2.2405\times10^{-4} \pm 3.80\times10^{-6}$	$3.1462\times10^{-4} \pm 1.66\times10^{-4}$
Total	$3.1587\times10^{-4} \pm 4.56\times10^{-6}$	$4.5574\times10^{-4} \pm 1.72\times10^{-4}$
Direct method	$3.3500\times10^{-4} \pm 1.96\times10^{-5}$	
Deterministic method	3.1018×10^{-4}	

Table 10. *k*-eigenvalue changes for light water density change (Case 4).

	PSM (C=20)	CS
Δk_{eff}^{NP}	$-7.7306\times10^{-7} \pm 5.53\times10^{-7}$	$-1.2908\times10^{-6} \pm 1.50\times10^{-6}$
Δk_{eff}^{PS}	$-1.0834\times10^{-4} \pm 2.20\times10^{-7}$	$-1.0825\times10^{-4} \pm 3.81\times10^{-6}$
Total	$-1.0911\times10^{-4} \pm 5.95\times10^{-7}$	$-1.0955\times10^{-4} \pm 4.10\times10^{-6}$
Direct method	$-1.3600\times10^{-4} \pm 2.19\times10^{-5}$	
Deterministic method	-1.0915×10^{-4}	

Table 11. Three group constants of graphite.

	1st group	2nd group	3rd group
$\Sigma_t\ (cm^{-1})$	0.23264	0.41793	0.42354
$\Sigma_c(cm^{-1})$	4.1681×10^{-5}	7.6738×10^{-6}	2.1311×10^{-4}
$\Sigma_{sg\to g}(cm^{-1})$	0.22122	0.41327	2.5313
$\Sigma_{sg\to g+1}(cm^{-1})$	0.011379	4.6514×10^{-3}	—

Table 12. *k*-eigenvalue changes for interface displacement by 1 cm (Case 5).

	PSM (C=3)	CS
Δk_{eff}^{NP}	$1.1793\times10^{-2} \pm 1.2\times10^{-5}$	—
Δk_{eff}^{PS}	$-7.7237\times10^{-3} \pm 9.6\times10^{-6}$	—
Total	$4.0692\times10^{-3} \pm 1.5\times10^{-5}$	—
Direct method	$4.0220\times10^{-3} \pm 2.16\times10^{-5}$	
Deterministic method	4.0182×10^{-3}	

Table 13. Relative figure-of-merit with respect to direct method. Number in parentheses denotes factor *C* in Eq. (32).

	Case 5	Case 6	Case 7	Case 8
Direct method	1	1	1	1
PSM	5.17 (C=1)	341 (C=1)	54.1 (C=1)	2.33×10^{5} (C=1)
	13.4 (C=3)	2114 (C=40)	301 (C=20)	7.20×10^{6} (C=3500)
	12.1 (C=5)	1479 (C=60)	241 (C=40)	6.00×10^{6} (C=5000)
CS	—	—	135	1.92×10^{4}

Table 14. *k*-eigenvalue changes for interface displacement by 0.02 cm (Case 6).

	PSM (C=40)	CS
Δk_{eff}^{NP}	$2.3001\times10^{-4} \pm 2.4\times10^{-7}$	—
Δk_{eff}^{PS}	$-1.4561\times10^{-4} \pm 8.3\times10^{-7}$	—
Total	$8.4398\times10^{-5} \pm 8.69\times10^{-7}$	—
Direct method	$4.40\times10^{-5} \pm 1.55\times10^{-5}$	
Deterministic method	8.3940×10^{-5}	

Table 15. *k*-eigenvalue changes for boundary extension by 3 cm (Case 7).

	PSM (C=20)	CS
Δk_{eff}^{NP}	$4.0950\times10^{-3} \pm 3.7\times10^{-6}$	$4.0875\times10^{-3} \pm 4.6\times10^{-6}$
Δk_{eff}^{PS}	$-1.2387\times10^{-3} \pm 3.5\times10^{-6}$	$-1.2572\times10^{-3} \pm 6.8\times10^{-6}$
Total	$2.8563\times10^{-3} \pm 5.1\times10^{-6}$	$2.8302\times10^{-3} \pm 8.2\times10^{-6}$
Direct method	$2.8810\times10^{-3} \pm 1.92\times10^{-5}$	
Deterministic method	2.8564×10^{-3}	

Table 16. *k*-eigenvalue changes for boundary extension by 0.02 cm (Case 8).

	PSM (C=3500)	CS
Δk_{eff}^{NP}	$3.3091\times10^{-5} \pm 2.3\times10^{-8}$	$3.3132\times10^{-5} \pm 3.34\times10^{-7}$
Δk_{eff}^{PS}	$-9.8679\times10^{-6} \pm 2.16\times10^{-8}$	$-1.0123\times10^{-5} \pm 5.08\times10^{-7}$
Total	$2.3223\times10^{-5} \pm 3.2\times10^{-8}$	$2.3009\times10^{-5} \pm 6.08\times10^{-7}$
Direct method	—	
Deterministic method	2.3790×10^{-5}	

Table 17. Dependence of *k*-eigenvalue change on spatial bin sizes in Case 2.

Spatial bins	(300+100+300)× (300+100+300)*	(15+5+15)×(15+5+5)	(7+3+7)×(7+3+7)
Δk_{eff}^{NP}	$5.2403\times10^{-3} \pm 8.6\times10^{-6}$	$5.2396\times10^{-3} \pm 8.5\times10^{-6}$	$5.1796\times10^{-3} \pm 8.2\times10^{-6}$
Δk_{eff}^{PS}	$5.1561\times10^{-3} \pm 6.8\times10^{-6}$	$5.1982\times10^{-3} \pm 6.8\times10^{-6}$	$5.1985\times10^{-3} \pm 2.4\times10^{-6}$
Total	$1.0396\times10^{-2} \pm 1.1\times10^{-5}$	$1.0438\times10^{-2} \pm 1.1\times10^{-5}$	$1.0378\times10^{-2} \pm 8.5\times10^{-6}$

*This is the same as in Table 6.

Table 17 (continued).

Spatial bins	(4+2+4)×(4+2+4)	(3+2+3)×(3+2+3)
Δk_{eff}^{NP}	$4.9725\times10^{-3} \pm 8.3\times10^{-6}$	$4.5344\times10^{-3} \pm 8.2\times10^{-6}$
Δk_{eff}^{PS}	$5.1395\times10^{-3} \pm 2.5\times10^{-6}$	$4.7738\times10^{-3} \pm 2.4\times10^{-6}$
Total	$1.0112\times10^{-2} \pm 8.7\times10^{-6}$	$9.3082\times10^{-3} \pm 8.5\times10^{-6}$